European Polymer Journal 239 (2025) 114273

Contents lists available at ScienceDirect

European Polymer Journal

journal homepage: www.elsevier.com/locate/europolj

Atomistic modeling of bond exchange reaction and self-healing mechanisms in epoxy vitrimers

Amin Kuhzadmohammadi, Ning Zhang *

Department of Mechanical Engineering, Baylor University, Waco, TX 76706, USA

ARTICLE INFO

Keywords:
Vitrimer
Dynamic bond exchange
Self-healing
Covalent adaptable networks (CANs)
Molecular dynamics simulation

ABSTRACT

Epoxy-based vitrimers represent a promising class of covalent adaptable networks that offer a sustainable alternative to traditional thermosets by combining structural robustness with reprocessability and intrinsic self-healing. However, the molecular-level mechanisms underlying these dynamic functionalities remain insufficiently understood. In this study, we develop a large-scale molecular dynamics framework to model the curing and bond exchange processes in vitrimers synthesized from diglycidyl ether of bisphenol A (DGEBA) and 4-aminophenyl disulfide (4-AFD). A custom curing algorithm enables the construction of crosslinked networks with controlled crosslink densities (ρ_{cl}), allowing us to systematically evaluate the impact of network topology on mechanical and thermal properties. Our simulations reveal that increasing ρ_{cl} enhances the glass transition temperature, elastic modulus, and ultimate strength, due to reduced segmental mobility and a denser network structure. Crucially, we show that the incorporation of dynamic disulfide bonds enables thermally activated bond exchange reactions that effectively heal both nanovoids and preexisting cracks. The self-healed vitrimer recovers over 95% of its original mechanical performance, demonstrating the efficacy of network reconfiguration at the atomic scale. These findings provide mechanistic insights into the interplay between network architecture and vitrimer functionalities that are inaccessible by experiment alone. Our computational framework offers predictive capabilities for guiding material design and optimizing vitrimer performance for recyclable, reprocessable, and damage-tolerant polymer systems.

1. Introduction

Polymers have become indispensable in various industrial applications, serving both as core materials and as matrix phases in composite structures due to their outstanding mechanical, thermal, and chemical properties [1]. Typically, polymers are categorized into thermoplastics and thermosets, each exhibiting significantly distinct characteristics [2]. Thermoplastics are well known for their reversible melting capabilities, facilitating easy processing, reshaping, and recycling [3,4]. Thermosets, in contrast, are characterized by extensive and irreversible cross-linked networks, which confer superior mechanical robustness, chemical resistance, and thermal stability [5]. These attributes make thermosets highly desirable for specialized applications in aerospace, automotive, marine, electronics, adhesives, and coating sectors [6–9].

Despite these advantages, the inherent irreversibility of conventional thermosets significantly restricts their recyclability, repairability, and sustainability [10]. This limitation poses considerable challenges regarding environmental sustainability, effective waste management, and long-term economic efficiency [11,12]. Additionally, traditional epoxy thermosets are predominantly derived from nonrenewable fossil resources, intensifying concerns related to resource depletion and increased carbon emissions [13,14]. Hence, addressing these issues through innovative solutions has become increasingly urgent.

Recent advances in dynamic covalent chemistry offer a promising pathway to address these constraints by integrating dynamic covalent bonds into thermosetting polymer networks, resulting in covalent adaptable networks (CANs), notably vitrimers [16]. These networks demonstrate the remarkable ability to undergo thermally activated bond exchange reactions (BERs), enabling reshaping, recycling, and self-healing without sacrificing mechanical integrity [16–21]. The foundational work of Chen et al.,employing thermally re-mendable cross-linked polymers through Diels–Alder linkages [22], and subsequent research by Montarnal et al. on transesterification-based vitrimers [18], have established the conceptual groundwork for these versatile materials. Among various dynamic chemistries, disulfide-based vitrimers have mainly gained prominence due to their moderate reaction conditions

* Corresponding author.
E-mail address: ning_zhang@baylor.edu (N. Zhang).

https://doi.org/10.1016/j.eurpolymj.2025.114273
Received 21 July 2025; Received in revised form 3 September 2025; Accepted 5 September 2025
Available online 8 September 2025

and efficient self-healing and recyclability [23–26].

Experimental validations have underscored the significant potential of disulfide-containing epoxy vitrimers. For instance, recyclable fiber-reinforced epoxy composites with exchangeable disulfide cross-links have been demonstrated [6]. Similarly, aromatic disulfide epoxy thermosets have shown efficient self-healing and shape-memory properties upon heating [27]. Additionally, self-healing properties have been further enhanced by integrating graphene oxide nanofillers into vitrimer matrices [25].

Complementing these experimental endeavors, molecular dynamics (MD) simulations have provided critical insights into the microscopic dynamics and mechanical responses of vitrimers. MD simulations incorporating dynamic crosslinking have been used to explore self-healing behaviors [28]. Other studies have investigated the progressive fatigue mechanisms in epoxy thermosets under cyclic deformation [29]. These computational efforts have significantly advanced the fundamental understanding of how atomic-scale components, molecular structures, and dynamic processes collectively influence and dictate the macroscopic performance of these materials. Nevertheless, considerable gaps remain in fully elucidating the molecular-level thermodynamics and kinetics underpinning bond exchange reactions, specifically their roles in governing self-healing. These gaps continue to hinder the full exploitation and optimization of vitrimers for high-performance engineering applications.

To address this crucial research gap, this study employs large-scale MD simulations to elucidate the detailed mechanisms of dynamic BERs in epoxy-based vitrimers synthesized from diglycidyl ether of bisphenol A (DGEBA) and 4-aminophenyl disulfide (4-AFD). We systematically examine the relationships between crosslink density (ρ_{cl}) and mechanical response, as well as characterize the self-healing behavior. Through controlled molecular damage and subsequent thermal treatment simulations, we rigorously evaluate the effectiveness of self-healing facilitated by dynamic disulfide exchange reactions. By addressing these specific aspects, our research provides crucial molecular-level insights for the rational design and optimization of vitrimers.

2. Molecular modeling and simulation setup

2.1. Vitrimer chemistry

DGEBA is one of the most commonly used epoxy resins, well known for its excellent mechanical strength, ease of processing, and well-understood molecular structure [30]. In this study, DGEBA serves as the base resin, while 4-aminophenyl disulfide (4-AFD) is used as the curing agent. The introduction of disulfide bonds via 4-AFD enables dynamic bond exchange reactions (BERs), which are thermally activated and reversible. These dynamic covalent bonds are crucial for imparting vitrimer functionalities such as self-healing, recyclability, and thermal malleability. Additionally, the aromatic structure of 4-AFD enhances the thermal and mechanical stability of the resulting network.

Vitrimers leverage multiple classes of dynamic covalent reactions, including transesterification, disulfide exchange, and imine-based exchanges, enabling tailored network structures and functional adaptability based on specific chemical mechanisms [31–35]. The crosslinking in the DGEBA/4-AFD vitrimer system investigated in this work is based on the classic epoxy–amine reaction: the primary amine on 4-AFD reacts with the epoxide group on DGEBA, leading to ring opening, formation of a C–N bond, and generation of a secondary alcohol. Each amine group on AFD can react with two epoxide groups, resulting in a highly crosslinked network. This DGEBA–AFD system thus provides an ideal platform for investigating the influence of crosslinking density and network architecture on the thermo-mechanical and dynamic properties of epoxy-based vitrimers. A schematic of the chemical structures and reactive sites of the monomers is provided in Fig. 1.

2.2. Model construction

The simulation workflow begins with the construction of an amorphous cell representing the uncrosslinked resin. An amorphous cell, comprising 298 DGEBA and 149 AFD monomers to reflect a stoichiometric 2:1 epoxide-to-amine ratio, was generated using the Amorphous Cell module in the Materials Studio software package [36]. The initial DGEBA-AFD system is shown in Fig. 2.

The polymer consistent force field (PCFF) [37], which has been

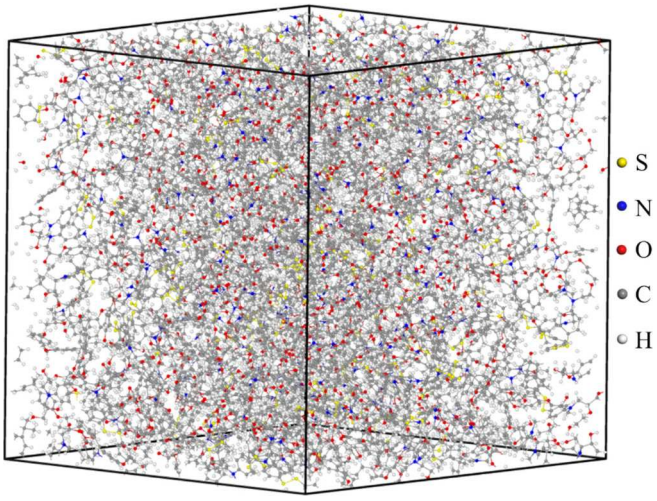

Fig. 2. Initial configuration of the uncrosslinked polymer network, constructed by randomly distributing a stoichiometric amount of DGEBA and 4-AFD molecules. Atom types are distinguished by color. This structure represents the precursor prior to curing reactions.

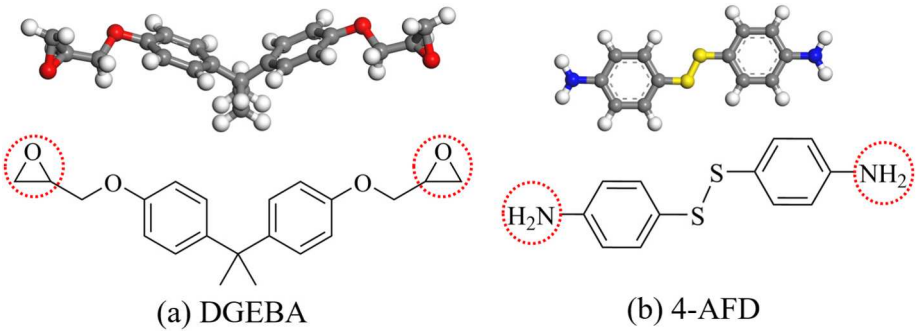

Fig. 1. Chemical structures of the monomers of (a) diglycidyl ether of bisphenol A (DGEBA) and (b) 4-aminophenyl disulfide (AFD). Red dashed circles highlight the reactive epoxide and amine groups responsible for crosslink formation.

widely used and validated for simulating polymers [38,39], was used to describe atomic interactions, including bonded terms (bond stretching, angle bending, dihedral and improper torsions) and non-bonded interactions modeled via Lennard-Jones and Coulombic potentials with a 10 Å cutoff. Prior to MD simulations, the monomer geometries were optimized using the conjugate gradient algorithm [40], and initial velocities were assigned according to a Maxwell–Boltzmann distribution at 300 K. The system then underwent a two-stage equilibration process. First, the structure was relaxed in the NPT ensemble at 300 K and 1 atm, allowing the simulation cell to compress or expand to reach the target density. Once the desired density was achieved and volume-induced stress was relieved, the simulation transitioned to the NVT ensemble to maintain a constant volume. Temperature regulation was achieved using a Nose–Hoover thermostat [41] to ensure a stable kinetic energy distribution. Upon completion of equilibration, the relaxed configurations were exported to LAMMPS [42,43] for cross-linking and further dynamic simulations. This modeling protocol provides a reliable and experimentally relevant starting point for subsequent vitrimer network formation and property analysis.

2.3. Cross-linking simulation

The formation of a polymer network from monomers in epoxy vitrimer systems proceeds via cross-linking, a process that fundamentally determines the final mechanical and thermal properties of the material. In MD simulations, this process typically involves two sequential stages: a "linking" stage, where monomers are covalently bonded based on proximity or energy criteria, and a "relaxation" stage, where high-temperature MD cycles relieve the artificially induced strain and promote network reorganization.

Due to computational constraints, atomistic MD simulations cannot replicate the long timescales and moderate temperatures used in experimental curing (e.g., ~140 °C for hours), where diffusion-limited reactions often lead to kinetic traps and heterogeneous network formation. To overcome this, simulations are typically performed at significantly elevated temperatures (e.g., 600–700 K) to accelerate molecular motion, enhance diffusion rates, and increase reaction probabilities, enabling high conversion levels (e.g., ~90 % cross-linking) within feasible simulation timescales of nanoseconds to microseconds. The selection of these temperatures was optimized to achieve a crosslink density comparable to experimental values (~85–95 % conversion in DGEBA/4-AFD systems [6]), while minimizing unphysical artifacts like bond strain. However, this high-temperature acceleration impacts the network structure by promoting more uniform topology and reduced heterogeneity compared to experimental conditions, where slower kinetics at lower temperatures can result in localized defects, chain entanglements, or incomplete reactions, leading to a more irregular and heterogeneous network. Consequently, simulated networks may exhibit slightly overestimated mechanical properties (e.g., 10–20 % higher modulus or strength) and T_g due to idealized homogeneity. Limitations include the potential oversight of temperature-dependent side reactions (e.g., oxidation or degradation not captured in classical MD) and the inability to model exact kinetic pathways, which restricts direct comparisons to equilibrium properties (e.g., density, T_g) rather than transient or defect-sensitive ones (e.g., fatigue or fracture behavior). Despite these disparities, the resulting network density and overall structure closely resemble those of experimentally cured epoxies, with the degree of curing quantified by the fraction of newly formed C–N bonds relative to the theoretical maximum, validating the approach for predictive material design.

3. Results and discussion

3.1. Curing reaction modeling

To model the curing process of the DGEBA–AFD vitrimer system, we employed a distance-based cross-linking algorithm that mimics the epoxy–amine reaction mechanism, as shown in Fig. 3a. Reactive centers were assigned to the epoxide carbon atoms of DGEBA and the amine nitrogen atoms of 4-AFD. Bond formation occurred when a reactive pair approached within a predefined cutoff distance, resulting in the creation of a C–N bond and implicit ring-opening of the epoxide group, as illustrated in Fig. 3b–e. The curing reaction proceeds through a two-step mechanism. First, a primary amine attacks the epoxide, generating a secondary amine and a hydroxyl group. The secondary amine can then further react with another epoxide to form a tertiary amine and an additional hydroxyl. Each nitrogen center is permitted to form up to two C–N bonds, while each epoxide carbon can react only once, consistent with the expected reaction stoichiometry.

To gradually achieve high cross-link density while preserving structural integrity, the reaction cutoff distance was incrementally increased by 0.5 Å in each cycle. After every round of new bond formation, the system was subjected to energy minimization and short NPT equilibration steps to redistribute local strain and maintain realistic network geometry. This process was repeated until the target ρ_{cl} of approximately 90 % was reached. Further details are provided in **Fig. S1**.

Following the completion of the cross-linking phase, the system was subjected to post-curing thermal annealing to eliminate residual stress and reach thermodynamic equilibrium. This was achieved through repeated heating and cooling cycles between 1 K and 600 K under NPT conditions (1 bar), with each cycle lasting 50 ps (See **Fig. S2**). Density convergence was used as an indicator of equilibration. This annealing step is particularly important in vitrimers, where stress relaxation and structural reorganization contribute to the long-term mechanical stability and are critical for accurately assessing dynamic bond exchange behavior, such as self-healing [44].

The curing process was monitored through the temporal evolution of cross-link formation, as monomers with reactive functional groups progressively formed new bonds and developed into a rigid network. As the simulation advanced, the system approached a quasi-equilibrium state with a stabilized ρ_{cl}. While the simulations focused on structural outcomes, it is important to note that real vitrimer curing is influenced by various kinetic factors such as temperature, mechanical stress, and the surrounding chemical environment [45], which modulate the rates of bond formation, cleavage, and exchange.

3.2. Crosslinked structure validation

Crosslinking density (ρ_{cl}) is a critical parameter governing the mechanical strength, thermal stability, and chemical durability of polymer networks [46–50]. A densely crosslinked structure restricts molecular mobility and reduces the presence of free chain ends, thereby enhancing the resistance to deformation and dissolution. In the DGEBA–AFD vitrimer system, the ability of each 4-AFD molecule to form up to four covalent bonds with epoxide groups enables the creation of a highly interconnected, load-bearing network.

To evaluate the formation and quality of the network, we analyzed the bonding configurations of 4-AFD molecules throughout the curing process. As shown in Fig. 4, the number of epoxide connections per 4-AFD molecule varies from zero to four, representing different levels of crosslinking saturation. Fully saturated 4-AFD units (four epoxide linkages) contribute most effectively to mechanical reinforcement, while underutilized molecules (with one to three linkages) represent network imperfections that may result in local flexibility and reduced load transfer efficiency.

Initially, a significant fraction of 4-AFD molecules remains unreacted, but as curing progresses, the population shifts toward higher degrees of connectivity. At intermediate conversion levels (20 %, 50 %, and 70 %), the fractions of 4-AFD molecules with one, two, and three linkages, respectively, reach their maximum. This reflects the progressive nature of bond formation and the emergence of a complex polymer

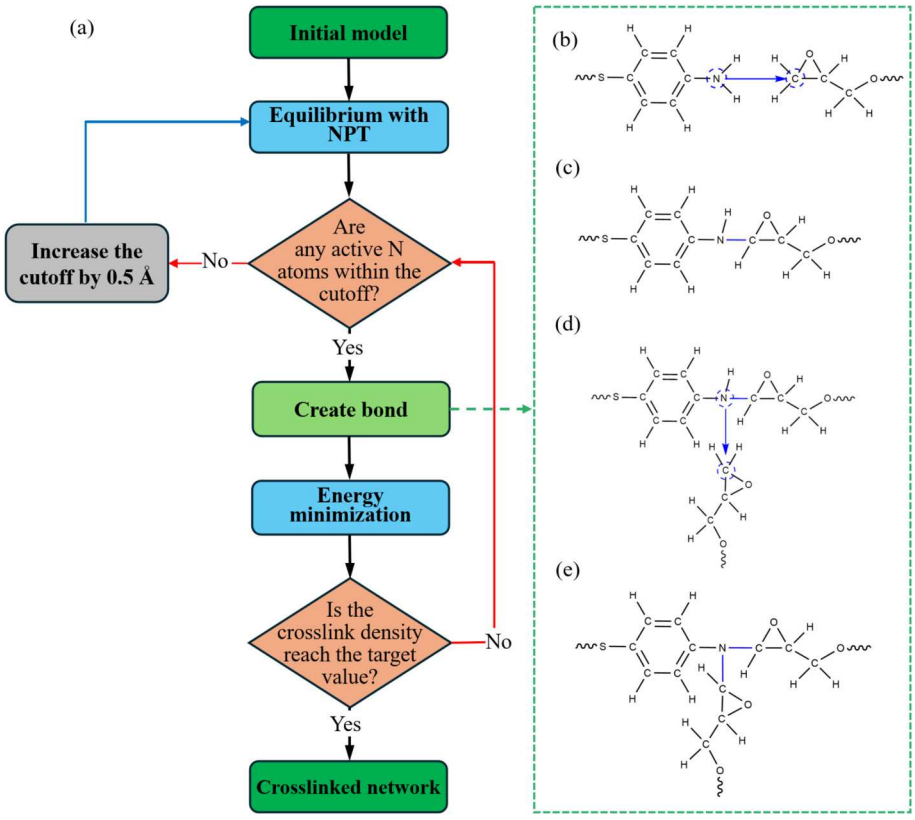

Fig. 3. (a) The curing algorithm between the epoxy resin and the amine curing agent is modeled as a stepwise mechanism. (b) Each epoxy group is initially attacked by a primary amine, (c) yielding a secondary amine and a hydroxyl group. (d) The secondary amine subsequently reacts with another epoxy group. (e) Generate a tertiary amine and a second hydroxyl group.

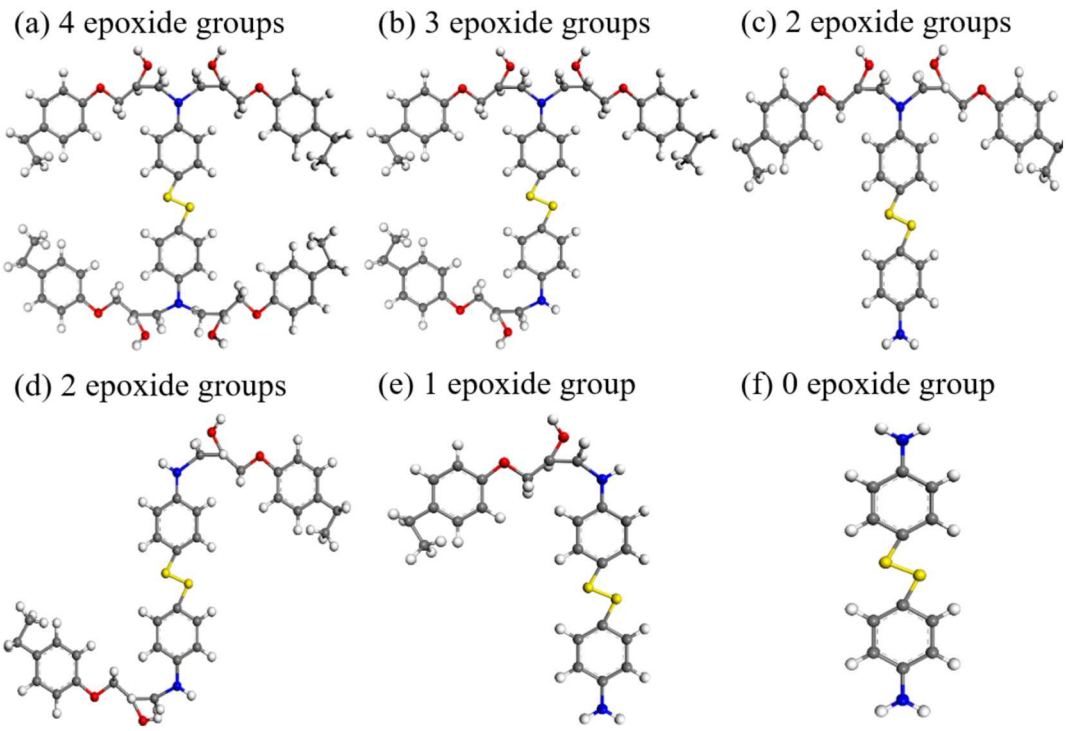

Fig. 4. Representative configurations illustrate the potential connectivity of a 4-AFD molecule with epoxide groups during curing. Subpanel (a–f) shows 4-AFD molecules bonded with 4, 3, 2, 1, or 0 epoxide groups, respectively, reflecting the possible crosslink states and network topologies in the cured vitrimer system.

network. When the conversion reaches 90 %, the crosslinked architecture becomes significantly more saturated: nearly all 4-AFD molecules participate in network formation, with ~65 % achieving full fourfold connectivity (Fig. 5). This high level of saturation indicates a robust network with enhanced stiffness and thermal resistance (Further computational details are provided in **Figs. S3–S6**).

The data obtained from our simulations show strong agreement with the predictions derived from statistical analysis. This correlation underscores the reliability of our models in capturing the interaction behavior between 4-AFD and epoxide groups during the crosslinking process. The accuracy of these models is crucial for designing polymers with tailored properties, as they allow for precise control of crosslinking density and network structure. The expected number of curing agents with four occupied active sites (E) is determined using the combinatorial framework [51]. The derivation proceeds as follows:

$$E = \sum_{i=1}^{N} P(\text{The ith curing agent isfully saturated}) \tag{1}$$

where N is the total number of curing agent molecules in the system, each with four independent active sites, and P represents the probability that a given curing agent has a specific number of active sites occupied, as defined by combinatorial arrangements. To evaluate the probability that a specific curing agent has all four sites occupied, we consider the selection of occupied sites among all available sites. The probability is given by:

$$P = \frac{C_4^4 C_{4N-4}^{4N_p-4}}{C_{4N_p}^{4N_p}} \tag{2}$$

where $C_n^k = \frac{n!}{k!\times(n-k)!}$ denotes binomial coefficient. Expanding the binomial coefficients yields:

$$E = N \times \frac{\frac{(4N-4)!}{(4N_p-4)!(4N-4N_p)!}}{\frac{4N!}{4N_p!(4N-4N_p)!}} \tag{3}$$

where p is the occupation fraction, the fraction of all active sites that are occupied ($0 \le p \le 1$). With further simplification, we have:

$$E = N_p \frac{(4N_p-1)(4N_p-2)(4N_p-3)}{(4N-1)(4N-2)(4N-3)} \tag{4}$$

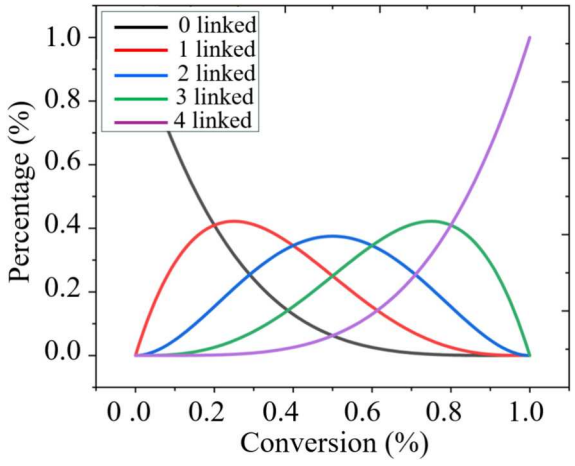

Fig. 5. Statistical distribution of 4-AFD molecules linked to 0, 1, 2, 3, or 4 epoxide groups at various curing stages, represented by different conversion percentages. The data quantifies the cross-linking evolution, with a marked decrease in unreacted 4-AFD molecules and a corresponding increase in highly linked molecules as curing proceeds, reflecting the formation of a denser polymer network.

These parameters provide a quantitative basis for characterizing the distribution of crosslinking states and evaluating network saturation at the molecular level. The expected number of curing agents with four occupied reactive sites is computed by multiplying the total number of curing agents by the combinatorial probability that all four sites are occupied, as described above. This framework accounts for the stochastic nature of site occupation in the network formation process and provides a quantitative measure of network saturation at the molecular level.

3.3. Glass transition temperature (T_g) prediction

T_g is a fundamental thermal property of polymers that marks the transition of polymers from a rigid, glassy state to a soft, rubbery state [52–54]. Below T_g, molecular mobility is significantly restricted, while above T_g, the chains gain sufficient thermal energy to move more freely, resulting in increased flexibility and elasticity [52,54]. This transition significantly affects the mechanical and thermal properties of polymers, making T_g an essential parameter for understanding and predicting the behavior of polymeric materials in various applications [55].

Understanding T_g is crucial for selecting suitable polymers for specific service conditions. For instance, polymers used in high-temperature environments must have a T_g above the operating temperature to maintain their structural integrity. Conversely, for applications that require flexibility and impact resistance at lower temperatures, polymers with a lower T_g are more suitable [56]. Thus, T_g plays a vital role in material selection and designing materials with desired properties.

The glass transition is typically accompanied by changes in physical properties, such as specific volume and density, as well as thermal and mechanical behavior. In MD simulations, T_g is usually obtained by analyzing variations in density or specific volume as a function of temperature. In this study, MD simulations were conducted in the NPT ensemble at a cooling rate of 1 K/ps to calculate T_g. The temperatures and densities of the models were recorded for further analysis. Fig. 6a shows temperature-dependent density curves for different crosslinking densities, and Fig. 6b presents the specific volume of the 90 % crosslinked system. A clear turning point in slope was observed around 390 K, which indicates the T_g and has a good alignment with reported values in the literature [6]. Below 390 K, the polymer exhibits a lower specific volume, indicative of a denser and more rigid structure. Above this temperature, the specific volume increases more rapidly, indicating a transition to a more flexible and less dense state. To accurately identify the T_g, a piecewise linear function was used to fit the temperature–density data.

3.4. Temperature-driven bond exchange

In this study, we modeled the dynamic bond exchange processes in a vitrimer system, recognizing that these reactions exhibit sluggish kinetics at ambient temperatures but accelerate significantly as the temperature approaches or exceeds the topological freezing transition temperature (T_v) of the vitrimer [57]. T_v is a crucial parameter for vitrimers, marking the threshold above which dynamic covalent bonds become highly active [58]. When the temperature exceeds T_v, the material exhibits significant bond exchange activity, enabling the network to flow and behave as a viscoelastic liquid [59]. This facilitates reprocessing, recycling, and self-healing capabilities. Conversely, below T_v, the exchange reactions are effectively frozen, and the vitrimer behaves as a rigid thermoset with limited molecular mobility [60]. Importantly, T_v generally occurs at temperatures above T_g, distinguishing the onset of dynamic network rearrangement from the transition between glassy and rubbery states [61]. Near T_v, the modulus of material decreases, and the mobility of polymer chains increases in a sigmoidal manner corresponding to a higher likelihood of transesterification or other bond exchange reactions. To capture this behavior, we implemented a temperature-dependent sigmoidal function centered at T_v to

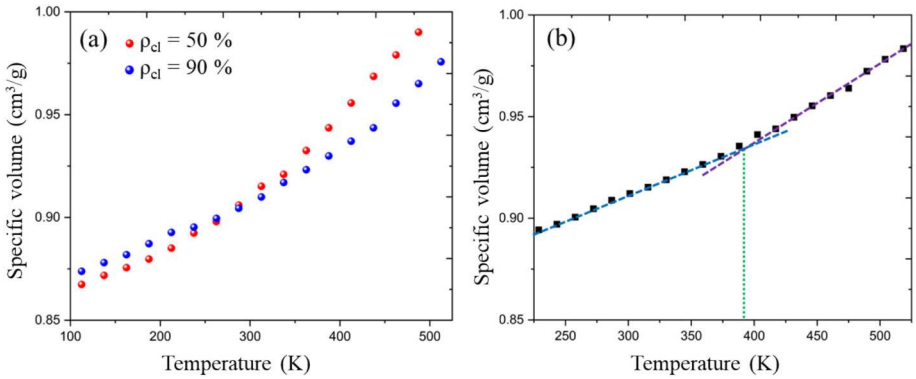

Fig. 6. (a) Specific volume as a function of temperature plot used to determine the glass transition temperature (T_g). (b) A noticeable turn point in slope was observed near 390 K for the system with ρ_{cl} = 90 %, indicating the onset of T_g.

enhance the kinetics of the bond exchange in our model.

Given that the experimentally observed time scales of bond exchange are relatively long, we accelerated the reaction rates in our MD simulations to effectively capture the thermomechanical behavior of the vitrimer within computationally feasible timeframes [62]. The dynamic bond exchange was represented using a two-step reaction framework, involving the pre- and post-reaction templates, along with a reaction map that governed exchange events. The temperature-dependent probability of the bond exchange, *p(T)*, was defined by the following sigmoidal equation [28]:

$$p(T) = \frac{1}{\exp\left(-a(T-T_v) - \ln\left(\frac{pT_v}{1-pT_v}\right)\right)+1}, \text{where } a = \frac{2pT_v}{w(1-pT_v)} \quad (5)$$

Here, *w* represents the width of the transition window around T_v. It is determined from the modulus-temperature relationship; in this study, we set w = 40 K. The parameter $pT_v = 0.9$ reflects the probability of bond exchange occurring at the transition temperature T_v, implying that a majority of exchange reactions occur around this point. At the onset of the transition window (i.e., T_v-*w*), the probability is $p(T_v\text{-}w) = 0.1$, ensuring a smooth increase in the reaction rate. When reactive sites, such as pairs of sulfur (S–S) atoms from different polymer chains, approach within a designated cutoff distance (4.12 Å, twice the typical S–S bond length of 2.06 Å), bond exchange reactions may occur. As temperature increases, the frequency of these reactions rises due to enhanced atomic mobility, reaching a maximum once the temperature surpasses T_v. This increase is primarily driven by the increased frequency of collision events between reactive atoms. Such a modeling approach aligns well with experimental observations and effectively captures the thermomechanical behavior of the vitrimer system under varying temperature conditions.

Fig. 7 depicts the influence of temperature on both the bond exchange probability and the total number of bond exchange reactions within the system. A clear trend is observed: as the temperature increases, the number of reactions also increases. Notably, surpassing the threshold temperature (T_v), the reaction probability reaches 1.0, indicating near-complete bond exchange activity. This phenomenon is attributed to the increased frequency of collisions among bonding atoms at elevated temperatures. These characteristics are obtained by formulating a reaction probability centered around the topological freezing transition point, informed by experimental data. We calculated $T_v = 410$ K as a reference point to assess the temperature-dependent probability of bond exchange reactions.

To elucidate the molecular mechanisms governing disulfide bond exchange in the DGEBA/4-AFD vitrimer system, we employed a sigmoidal probability model, centered at the topological freezing transition temperature $T_v = 410$ K, with a transition window width w = 40. The temperature sensitivity of disulfide exchange in our sigmoidal

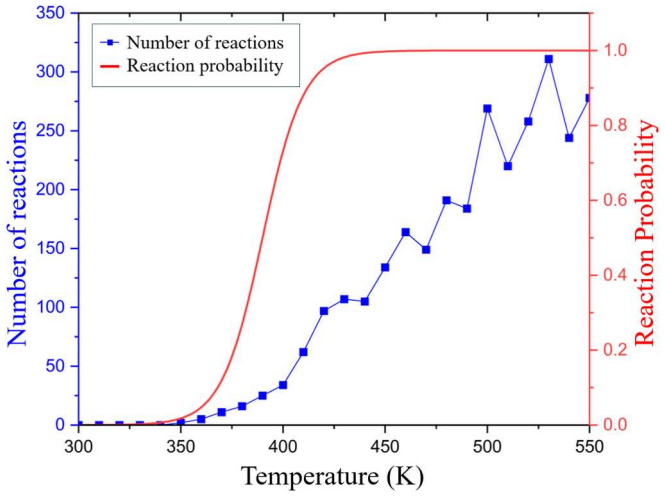

Fig. 7. Temperature dependence of the reaction probability (right vertical axis) for dynamic disulfide exchange and the corresponding number of S–S bond rearrangements (left vertical axis). The reaction probability features a sigmoidal increase near T_v, highlighting the sharp enhancement in bond exchange activity at elevated temperatures.

model is consistent with reported activation energies for aromatic disulfide metathesis. Quantum chemical (DFT) and experimental studies have estimated the activation energy (E_a) of disulfide bond exchange to be in the range of 50–70 kJ/mol [63–65]. According to transition state theory, the reaction rate follows the Arrhenius equation, which is

$$k = A\exp(-\frac{Ea}{RT}) \quad (6)$$

where at T_v = 410 K, the thermal energy ($RT \cong 3.4 kJ/mol$) enables a significant fraction of molecules to surpass the energy barrier, resulting in a high bond exchange probability ($pT_v = 0.9$). This is consistent with experimental observations of stress relaxation in disulfide-based vitrimers, with relaxation times decreasing from 3 h at 130 °C to 20 s at 200 °C, enabling efficient reprocessability and self-healing at elevated temperatures [6]. The sigmoidal model effectively approximates the rapid increase in reaction rate near T_v, driven by enhanced molecular collisions, although external mechanical stimuli can further modulate the effective barrier, as indicated by DFT studies on similar disulfide systems. However, the classical MD framework simplifies quantum mechanical transition states, potentially underestimating local steric or electronic effects, which could be addressed in future quantum–classical hybrid simulations. The sigmoidal model thus provides a phenomenological yet effective representation of the rapid increase in bond

exchange activity near T_v, driven by enhanced molecular mobility and collisions. While mechanical stimuli and local steric or electronic effects may further modulate the effective barrier—as suggested by DFT studies—these subtleties are not fully captured in a classical MD framework. Incorporating quantum–classical hybrid approaches in future work could help address such limitations and refine the accuracy of reaction dynamics in vitrimers.

3.5. Effect of crosslink density (ρ_{cl}) on mechanical behavior

Crosslink density (ρ_{cl}) plays a crucial role in determining the mechanical behavior of amorphous polymers, including vitrimers [66,67]. To understand this impact, five polymer samples with varying crosslink densities, ranging from 50 % to 90 %, were constructed and subjected to tensile loading. Each sample was first relaxed for 1 ns at 300 K under atmospheric pressure, followed by a uniaxial tension test with a strain rate of 10^9/s. The resulting stress–strain responses, presented in Fig. 8, reveal clear trends correlating ρ_{cl} with the mechanical performance of vitimers.

As ρ_{cl} increases, the peak stress rises accordingly, indicating that polymers with a higher ρ_{cl} enhance the resistance of the material to mechanical deformation. Specifically, the sample with ρ_{cl} = 90 % exhibited the highest peak stress (~160 MPa), while samples with ρ_{cl} values of 80 %, 70 %, 60 %, and 50 % showed progressively lower peak stresses. This trend is attributed to the increased number of covalent crosslinks at higher ρ_{cl}, which restricts the movement of polymer chains, thereby enhancing network strength and rigidity.

Further analysis, depicted in **Fig. S7**, illustrates the dependence of Young's modulus, yield stress, and ultimate stress on ρ_{cl}. Young's modulus, a measure of material stiffness, exhibits a positive correlation with ρ_{cl}, as higher densities limit chain mobility and form more rigid, load-bearing networks [66,68]. These results align well with both MD predictions and experimental measurements, such as the reported modulus of 2.4 GPa for similar epoxy systems [6]. At low crosslink densities (e.g., 50 %), polymer chains retain considerable flexibility, allowing for more sliding and deformation, which results in reduced stiffness and lower Young's modulus values. As the density increases to intermediate levels (60–70 %), the network becomes increasingly rigid, improving load transfer and stress distribution. At high crosslink densities (80–90 %), the material becomes significantly stiffer and more brittle, with a tightly crosslinked architecture that strongly resists deformation and yields the highest Young's modulus among the considered samples.

Table 1
Comparison of simulated and experimental thermomechanical properties of the studied vitrimer.

Property	This work	Experiment [6]	Experiment [15]68]
T_g (°C)	117 °C	130 °C (DSC) 127 °C (DMA)	131 °C (DSC)
Young's Modulus (GPa)	2.2 GPa	2.6 GPa (DMA at 25 °C)	3.03 ± 0.03 GPa (tensile test, ASTM D638)
Tensile Strength (MPa)	155 MPa	88 MPa (at 7.1 % strain)	92.8 ± 0.2 MPa

As summarized in Table 1, the simulated results from this work show good alignment with experimental data for the DGEBA/4-AFD epoxy vitrimer system, with Tg values of 117 °C closely matching the reported 130–131 °C (DSC) and 127 °C (DMA) from experiments, confirming the model's ability to predict thermal transitions despite a slight underestimation due to idealized simulation conditions and accelerated kinetics. Young's modulus (2.2 GPa) aligns well with experimental ranges of 2.6–3.0 GPa (DMA/tensile), validating enhanced stiffness from crosslink density, while tensile strength is overestimated in simulations (155 MPa vs. 88–93 MPa experimentally) owing to the absence of real-world defects, voids, or heterogeneity; overall, these alignments substantiate the MD framework's predictive accuracy for material design.

3.6. Mechanism and kinetics of bond exchange

To accurately capture the self-healing behavior of vitrimers in MD simulations, it is essential to incorporate a mechanism that mimics the dynamic exchange of covalent bonds. In this work, a BER algorithm was implemented to replicate the associative bond-swapping characteristic of disulfide-based vitrimer networks. The core principle of this BER algorithm is to simulate the continuous breaking and reforming of disulfide bonds, enabling polymer network reconfiguration while maintaining the overall ρ_{cl} [25].

The BER algorithm operates by iterative "bond break/create" cycles, beginning with an initially well-crosslinked polymer network (90 %) equilibrated at 300 K to ensure structural stability. During each cycle, a substantial fraction of existing disulfide bonds, 80 %, are randomly broken, generating free sulfur atoms that serve as reactive sites. This random selection is crucial to avoid any bias in network topology and to provide opportunities for the network to explore new configurations. The 80 % break probability was tuned for DGEBA-AFD to achieve

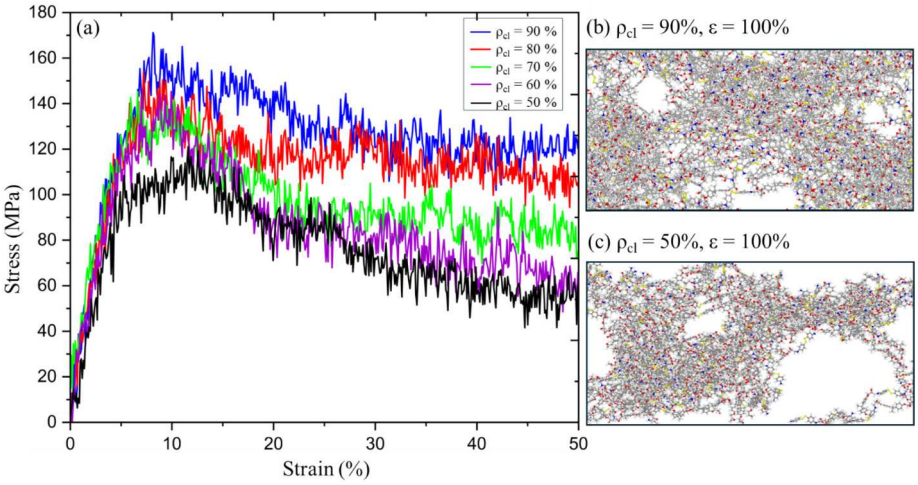

Fig. 8. (a) Stress–strain curves of vitrimer systems with varying ρ_{cl} (50 % to 90 %) subjected to uniaxial tension at 300 K. (b) Deformed configuration of the vitrimer with ρ_{cl} = 90 % at a strain of 100 %, showing a well-connected network. (c) Configuration with ρ_{cl} = 50 % at the same strain, revealing increased disruption and larger void formation.

healing efficiencies of more than 95 %. Lower probabilities (e.g., 50 %) underpredict healing; higher probabilities (90 %) cause unphysical network disruption.

Following the bond-breaking phase, the algorithm initiates a bond formation phase, in which new disulfide bonds are created between available sulfur atoms. To ensure a realistic representation of bond dynamics and to prevent the immediate reformation of previously broken pairs, a distance criterion is applied. Only when two unbonded sulfur atoms fall within a cutoff distance of 4.12 Å, then they are eligible to form a new bond. For each eligible pair, a new S–S bond is formed with a probability of 50 %. This probability-based approach is key to capturing the stochastic nature of chemical reactions and ensuring the diversity of crosslinking patterns throughout the simulation.

To govern the number of bond-breaking and bond-forming operations, two parameters, commonly denoted as "*a*" and "*b*". In this study, $a = 10$ (the total bond cuts in the BER loop) and $b = 50$ (the maximum number of bond formation attempts per cycle) were chosen. These values are selected based on prior work to balance computational efficiency with the need for thorough network rearrangement, and they can be adjusted according to the degree of healing or network evolution desired in the simulation [25]. Between each bond-breaking and bond-formation phase, the system undergoes a relaxation period, allowing polymer chains and reactive sites to diffuse and reposition, thus further enhancing the probability of successful crosslinking.

The effectiveness of the BER algorithm is particularly evident when simulating the healing process of a damaged vitrimer. A controlled "cut" is introduced by selectively breaking backbone bonds in a localized region of the polymer network. The BER algorithm then enables reformation of new disulfide bonds across the damaged interface, restoring structural connectivity and facilitating recovery of mechanical integrity. This healing process is highly temperature-dependent, as elevated temperatures enhance atomic mobility and thus accelerate both bond breaking and reforming, which thereby enhances the healing rate. Throughout the simulation, the total number of disulfide bonds may fluctuate slightly, but it remains close to the original value, reflecting the associative mechanism of bond exchange that distinguishes vitrimers from dissociative dynamic networks.

By carefully tuning the parameters that govern the BER algorithm, specifically, the probabilities of bond breaking and formation, the cutoff distance for new bond formation, and the numbers of cycles and attempts, the simulation can accurately mimic and reproduce the dynamic network restructuring and self-healing phenomena observed experimentally in vitrimers. This modeling approach not only allows for quantitative evaluation of healing efficiency and mechanical recovery but also provides molecular-level insights into how variations in network architecture, temperature, and nanofiller content can influence the dynamic response of these advanced polymer systems.

The flowchart in Fig. 9 illustrates an iterative algorithm designed to simulate the dynamics of disulfide bond exchange within a polymer network, which is implemented in LAMMPS. The process starts by initializing the molecular structure and setting two counters, *a* and *b*, to zero. The optimal values and tuning of these parameters were investigated by Park et al. [25]. The system is first equilibrated for 10,000 steps under the NVT ensemble. In each cycle of the algorithm, existing disulfide (S-S) bonds are evaluated with an 80 % probability of being broken; each successful bond cleavage increments counter *a* by one. Following the bond-breaking phase, counter *b* is reset to zero, and a 50 % probability is applied to form new disulfide bonds between available sulfur sites, incrementing *b* with each new bond created.

The dynamic disulfide bond exchange process in polymer networks is governed by the spatial proximity of reactive groups. When the distance between two S-S bonds from different polymer chains decreases below 4.2 Å, the system reaches a configuration that facilitates bond exchange. This process begins with the cleavage of the original S-S bonds,

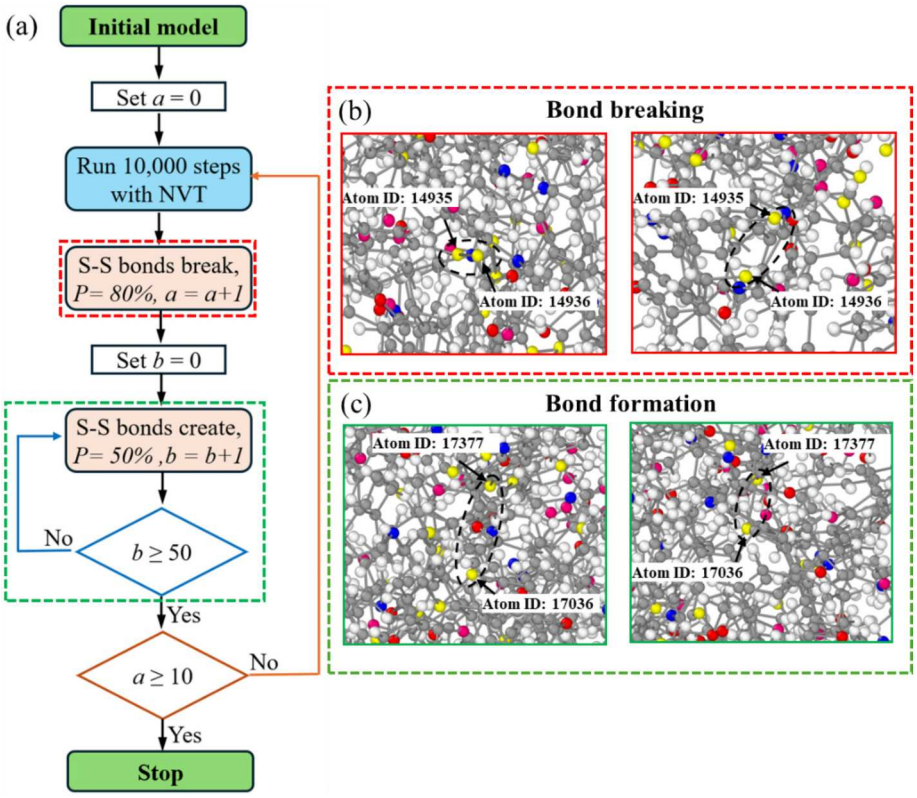

Fig. 9. (a) Flowchart of the "bond break/create" algorithm used to model disulfide bond exchange. The iterative procedure involves: (b) identifying existing S–S bonds that are probabilistically cleaved under specific probabilities. (c) subsequent formation of a new S–S bond with a neighboring chain. The iterative procedure involves probabilistic cleavage and reformation of S–S bonds, facilitating network rearrangement and enabling the modeling of self-healing behavior.

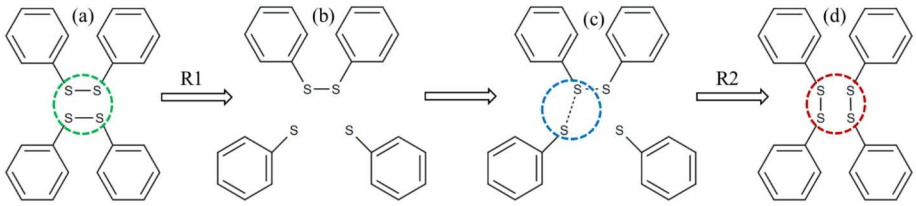

Fig. 10. Schematic representation of the two-step dynamic disulfide bond exchange reactions: (a, b) cleavage of an existing S-S bond in R1 and (c, d) formation of a new S-S bond through bond exchange in R2.

producing free sulfur atoms. Subsequently, the exchange proceeds through two sequential reactions: in Reaction (1) (R1), a sulfur atom from one chain forms a new bond with a sulfur atom from a different chain. Reaction (2) (R2) follows, wherein the remaining free sulfur atoms from different chains also bond, completing the exchange cycle.

Fig. 10 schematically depicts the bond exchange process. It begins with an initial disulfide bond, highlighted within a green dashed circle. Upon cleavage, the sulfur atoms become available to form new bonds. The left-hand sulfur atom forms a new S-S bond with the sulfur atom on a different chain, as indicated by a blue dashed circle. This is followed by a similar reaction involving the left-hand sulfur atom, thereby completing the disulfide bond exchange and forming new crosslinks (red dashed circle in Fig. 10).

3.7. Temperature effects on bond exchange

This study explores S-S BERs in a vitrimer polymer matrix under two different temperature conditions, 400 K, which is near T_v, and 450 K, which is above T_v, to assess the influence of thermal energy on reaction dynamics. The BERs proceed through two distinct mechanisms: Reaction (1) (R1) and Reaction (2) (R2). The progression of these reactions is quantified using the BER, which is tracked as a function of time (t), measured in nanoseconds (ns), capturing the rate and sequence of R1 and R2 throughout the simulation. As illustrated in Fig. 11, the BER curves clearly demonstrate a strong temperature dependence of the bond exchange process. Both R1 and R2 exhibit significantly higher reaction rates at 450 K compared to 400 K, indicating that elevated thermal energy facilitates faster bond cleavage and reformation by overcoming activation barriers more readily. R1 progresses more rapidly than R2 at both temperatures, suggesting that the initial formation of new S–S bonds is kinetically more favorable. The near-linear increase in BER over time reflects steady-state reaction kinetics, with steady-state conditions reached more quickly at higher temperatures due to enhanced molecular mobility and collision frequency.

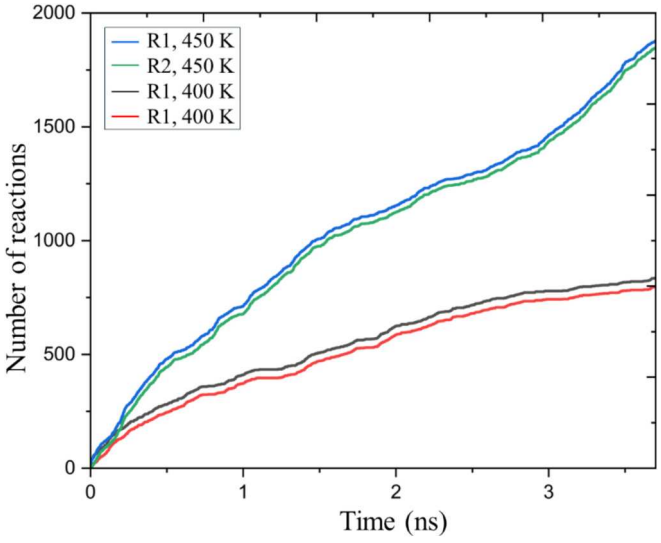

Fig. 11. BER curves as a function of time for R1 and R2 at two temperatures (400 K and 450 K). Elevated temperature significantly accelerates the bond exchange process, as evidenced by the steeper slopes for both reaction pathways at 450 K compared to 400 K.

These findings provide important molecular-level insights into the dynamic behavior of sulfur-containing vitrimer systems. Understanding the temperature sensitivity of bond exchange kinetics is crucial for designing responsive polymer networks with tunable mechanical properties, self-healing capability, and thermal reprocessability tailored to diverse industrial applications.

3.8. Crack self-healing

Traditional composites, while exhibiting tailored stiffness and strength, are often limited in their ability to autonomously recover from crack or notch-induced damage [69]. Self-healing capabilities provide a promising way to overcome such limitations by enabling the recovery of mechanical properties after damage through thermally activated bond exchange reactions. This is a critical functionality in vitrimers, enabling the autonomous repair of damage and thereby extending the lifespan of the material while maintaining its mechanical integrity. This self-healing behavior in vitrimers is attributed to the dynamic nature of sulfur-sulfur (S-S) bonds, which undergo reversible exchange reactions when thermally activated. Upon heating, these bonds rearrange, allowing the polymer network to reconfigure and restore continuity at damaged sites.

To explore the self-healing mechanism, a controlled crack with a width of 10 Å was introduced by severing central S-S bonds in the polymer network, simulating structural damage (Fig. 12). This model served as the damaged state for subsequent analysis. To assess recovery, MD simulations were conducted under two scenarios: one without dynamic S–S bond exchange (damaged) and one with the bond exchange mechanism activated (healed).

The healing process was initiated by heating the vitrimer to 450 K for 250 ps, enabling dynamic disulfide bond exchange, followed by cooling and relaxation to 300 K. After thermal treatment, the vitrimer regained its mechanical integrity. Tensile tests were performed to evaluate the stress–strain behavior across three states: pristine, damaged, and healed.

As shown in Fig. 13a, the pristine vitrimer exhibits a typical elastic–plastic response, characterized by a high Young's modulus of approximately 2.2 GPa and an ultimate tensile strength of 155 MPa. In sharp contrast, the damaged vitrimer, in which a central network crack is introduced, displays a markedly reduced Young's modulus of 0.9 GPa and a tensile strength of only 60 MPa, reflecting the substantial loss of network connectivity and mechanical integrity. Following the healing process enabled by dynamic disulfide bond exchange, the vitrimer demonstrates significant mechanical recovery. The healed model achieves a Young's modulus of 2.1 GPa and an ultimate tensile strength of 150 MPa. These values represent a recovery of over 95 % of the original stiffness and the tensile strength relative to the pristine sample. This near-complete restoration of mechanical performance provides compelling molecular-level evidence that dynamic bond exchange reactions can effectively re-establish both the elastic and strength properties of epoxy vitrimer networks after damage. Such high healing efficiency underscores the potential of disulfide-based vitrimers for use

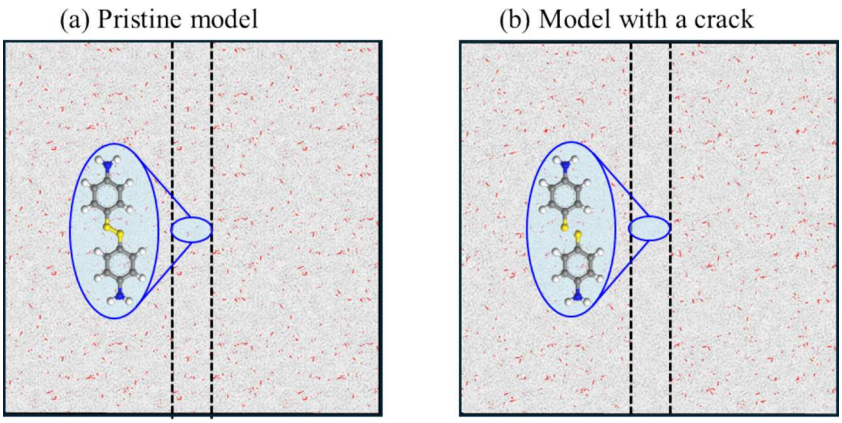

Fig. 12. Illustration of a "crack" introduced by deleting the sulfur-sulfur bond in the region between the two black dashed lines, as illustrated in the insets to mimic a localized damage. By breaking one link in the network, the capability for self-healing via bond exchange can be tested.

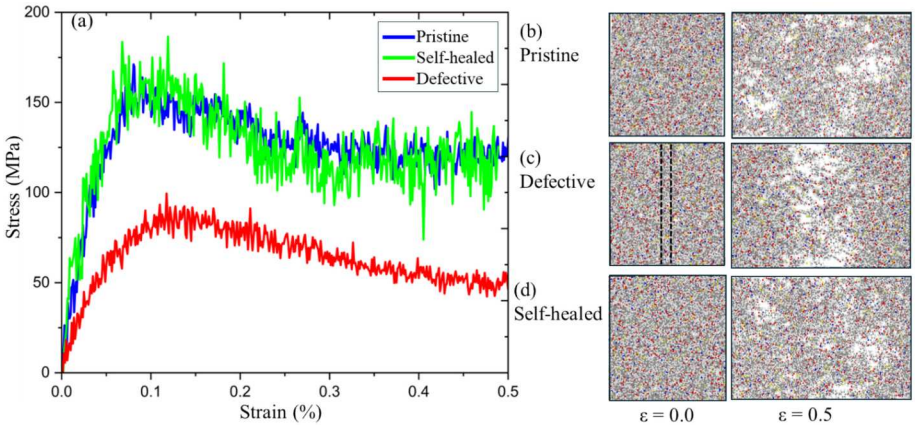

Fig. 13. (a) Stress–strain curves of the vitrimer in pristine, defective (with a 10 Å-wide crack), and thermally self-healed states under uniaxial tension at 300 K. The self-healed vitrimer recovers over 95 % of the original mechanical performance after thermal activation of dynamic bond exchange. (b–d) Representative molecular snapshots at strains of 0.0 and 0.5 for each condition, highlighting the restoration of network connectivity in the self-healed state compared to pronounced voids and disrupted connectivity in the damaged state.

in durable, self-healing polymeric materials for advanced structural applications.

The molecular configurations of the vitrimer in pristine, defective, and self-healed states across different levels of tensile deformation were compared in Fig. 13b-d. These structural snapshots complement the mechanical analysis by illustrating the microstructural evolution under deformation. In the pristine state, the polymer network remains continuous and well-connected, enabling uniform deformation and effective stress distribution. The damaged model, featuring an introduced 10 Å-wide crack, exhibits pronounced voids and network discontinuities, as indicated by the white regions representing broken bonds. This localized structural failure leads to stress concentration along the crack and results in premature fracture under loading.

In contrast, the healed vitrimer shows a reformed and more homogeneous network structure after thermal activation of dynamic disulfide exchange. The bond distribution is restored, and the voids present in the damaged state are largely eliminated. Notably, both the pristine and healed models display more uniform deformation and fracture behavior throughout the entire structure, while the damaged model exhibits localized failure along the pre-existing crack due to stress concentration. These visualizations reinforce the conclusion that dynamic bond exchange effectively restores the vitrimer's structural integrity and mechanical performance following damage.

3.9. Nanovoid self-healing

To further investigate the self-healing capability of vitrimers under severe damage conditions, a cylindrical through-hole defect was introduced into the polymer matrix using a strategy adapted from previous studies [70,71]. Specifically, A single-walled carbon nanotube (CNT) with a radius of 10 Å and a length of 60 Å, positioned along the out-of-plane direction, was embedded to delineate the void geometry. After curing and equilibration, the CNT was removed, creating a well-defined cylindrical hole that extended through the thickness of the vitrimer model. Subsequently, the damaged system was then annealed at 450 K for 250 ps to activate dynamic S–S bond exchange and promote network reformation. Following thermal treatment, the system was cooled and equilibrated at room temperature for mechanical evaluation. Fig. 14 presents a sequence of snapshots taken during the healing process. The images clearly show the progressive closure of the cylindrical void as the dynamic S–S bonds reconfigure, resulting in a reconstructed and continuous polymer network, further supporting the effectiveness of vitrimer-based self-healing strategies (A video illustrating the healing process is provided in the SI).

The mechanical response and failure modes of the pristine, defective, and healed vitrimer were illustrated in Fig. 15a. The stress–strain curves show that the healed vitrimer exhibits a substantial recovery in mechanical performance compared to the void-containing case. Notably, the stiffness of the healed vitrimer matches that of the pristine sample,

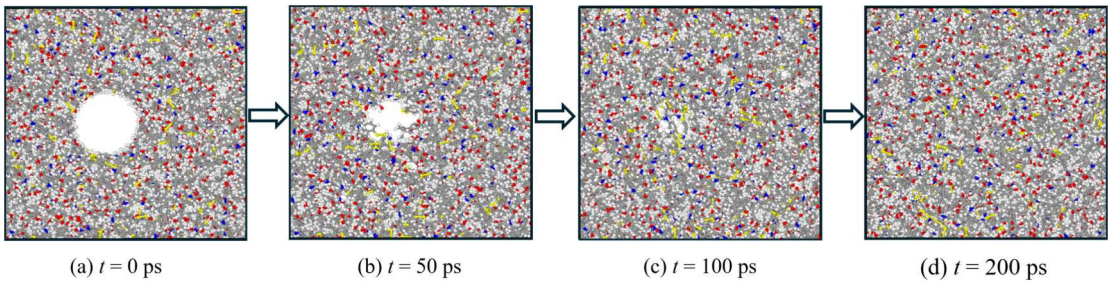

Fig. 14. Sequential molecular snapshots during the self-healing of a cylindrical void in the vitrimer network at relaxation times of (a) 0 ps, (b) 50 ps, (c) 100 ps, and (d) 200 ps. The images illustrate progressive closure of the defect via dynamic S–S bond exchange and network reconfiguration under thermal activation.

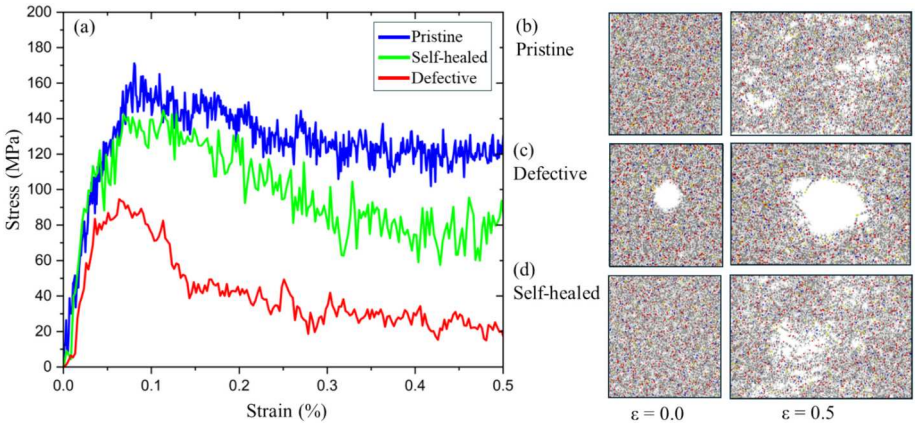

Fig. 15. (a) Stress–strain curves of the vitrimer in pristine, void-introduced, and thermally healed states under uniaxial tension at 300 K, illustrating the mechanical recovery achieved through dynamic bond exchange. (b–d) Corresponding molecular snapshots at selected strain levels, showing (b) the intact network in the pristine sample, (c) disrupted connectivity and void growth in the damaged sample, and (d) restored structural integrity in the self-healed system.

indicating a full recovery of elastic properties. Although the ultimate strength is slightly reduced, this can be reasonably attributed to the removal of a substantial number of atoms during the creation of the cylindrical defect, which lowers the total load-bearing capacity. Despite this, the healed vitrimer exhibits uniform deformation and delayed fracture, highlighting the effectiveness of dynamic disulfide bond exchange in restoring structural integrity and mechanical resilience. Visual comparisons in Fig. 15b-d of the failure modes reveal that the pristine and healed systems undergo uniform deformation and delayed fracture, whereas the void-containing sample fails prematurely along the defect site.

4. Conclusions

In this work, we developed a comprehensive MD framework to uncover the molecular-level mechanisms governing curing, deformation, and self-healing in epoxy-based vitrimers. By implementing a novel algorithm to simulate crosslink formation and dynamic disulfide bond exchange, we constructed polymer networks with controlled ρ_{cl} and systematically quantified their mechanical and thermal responses. Our findings reveal that increased ρ_{cl} enhances stiffness, strength, and glass transition temperature by forming denser, more rigid networks, while the presence of cracks or voids severely degrades mechanical integrity due to disrupted connectivity.

Importantly, we demonstrate that thermally activated disulfide bond exchange enables efficient network reconfiguration and repair. The vitrimer recovers over 95 % of its original Young's modulus and tensile strength following self-healing, as evidenced by the restored stress–-strain behavior and the closure of nanoscale damage. These results provide direct, atomistic-level validation of associative bond exchange as a powerful mechanism for healing damage in vitrimer systems, which are capabilities that remain difficult to resolve experimentally.

Beyond revealing critical structure–property relationships, this study contributes a predictive computational toolset to guide the rational design of recyclable, reprocessable, and damage-tolerant polymers. By offering mechanistic insight into bond exchange and network evolution, our work bridges the gap between molecular simulation and experimental vitrimer development. Future efforts will focus on optimizing network topologies, exploring alternative dynamic chemistries, validating simulation predictions through experimental collaboration, as well as integrating machine learning techniques to accelerate the screening and discovery of vitrimer formulations with tailored performance.

CRediT authorship contribution statement

Amin Kuhzadmohammadi: Writing – original draft, Visualization, Validation, Software, Methodology, Formal analysis. **Ning Zhang:** Writing – review & editing, Supervision, Project administration, Methodology, Funding acquisition, Conceptualization.

Declaration of competing interest

The authors declare that they have no known competing financial interests or personal relationships that could have appeared to influence the work reported in this paper.

Acknowledgments

This work was supported by the National Science Foundation under Award Numbers DMR-2316676 and CMMI-2302981. Simulations were performed at the ACCESS national supercomputer center.

Appendix A. Supplementary data

Supplementary data to this article can be found online at https://doi.org/10.1016/j.eurpolymj.2025.114273.

Data availability

The data that support the findings of this study are available from the corresponding author upon reasonable request.

References

[1] N.M. Nurazzi, M. Asyraf, A. Khalina, N. Abdullah, H. Aisyah, S.A. Rafiqah, F. Sabaruddin, S. Kamarudin, M. Norrrahim, R. Ilyas, A review on natural fiber reinforced polymer composite for bullet proof and ballistic applications, Polymers 13 (4) (2021) 646.

[2] E. Saldívar-Guerra, E. Vivaldo-Lima, Introduction to polymers and polymer types, Handbook of Polymer Synthesis, Characterization, and Processing (2013) 1–14.

[3] M. Biron, Thermoplastics and Thermoplastic Composites, William Andrew, 2018.

[4] A. Bîrcă, O. Gherasim, V. Grumezescu, A.M. Grumezescu, Introduction in thermoplastic and thermosetting polymers, Mater. Biomed. Eng. Elsevier (2019) 1–28.

[5] M. Biron, Thermosets and Composites, Elsevier, 2003.

[6] A.R. de Luzuriaga, R. Martin, N. Markaide, A. Rekondo, G. Cabañero, J. Rodríguez, I. Odriozola, Epoxy resin with exchangeable disulfide crosslinks to obtain reprocessable, repairable and recyclable fiber-reinforced thermoset composites, Mater. Horiz. 3 (3) (2016) 241–247.

[7] S. Paolillo, R. Bose, M. Santana, A. Grande, Intrinsic self-healing epoxies in Polymer Matrix Composites (PMCs) for aerospace applications, Polymers 13 (2021) 201.

[8] Q. Guo, Thermosets: Structure, Properties, and Applications, Woodhead Publishing, 2017.

[9] D. Ratna, Recent advances and applications of thermoset resins, 2022.

[10] W. Post, A. Susa, R. Blaauw, K. Molenveld, R.J. Knoop, A review on the potential and limitations of recyclable thermosets for structural applications, Polym. Rev. 60 (2) (2020) 359–388.

[11] D.J. Fortman, J.P. Brutman, G.X. De Hoe, R.L. Snyder, W.R. Dichtel, M.A. Hillmyer, Approaches to sustainable and continually recyclable cross-linked polymers, ACS Sustain. Chem. Eng. 6 (9) (2018) 11145–11159.

[12] S.V. Wanasinghe, O.J. Dodo, D. Konkolewicz, Dynamic bonds: adaptable timescales for responsive materials, Angew. Chem. 134 (50) (2022) e202206938.

[13] F. Ng, G. Couture, C. Philippe, B. Boutevin, S. Caillol, Bio-based aromatic epoxy monomers for thermoset materials, Molecules 22 (1) (2017) 149.

[14] A. Samir, F.H. Ashour, A.A. Hakim, M. Bassyouni, Recent advances in biodegradable polymers for sustainable applications, npj Mater. Degrad. 6 (1) (2022) 68.

[15] V. Schenk, J. De Calbiac, R. D'Elia, P. Olivier, K. Labastie, M. Destarac, M. Guerre, Epoxy vitrimer formulation for resin transfer molding: Reactivity, process, and material characterization, ACS Appl. Polym. Mater. 6 (10) (2024) 6087–6095.

[16] C.J. Kloxin, T.F. Scott, B.J. Adzima, C.N. Bowman, Covalent adaptable networks (CANs): A unique paradigm in cross-linked polymers, Macromolecules 43 (6) (2010) 2643–2653.

[17] A.V. Karatrantos, O. Couture, C. Hesse, D.F. Schmidt, Molecular simulation of covalent adaptable networks and vitrimers: A review, Polymers 16 (10) (2024) 1373.

[18] D. Montarnal, M. Capelot, F. Tournilhac, L. Leibler, Silica-like malleable materials from permanent organic networks, Science 334 (6058) (2011) 965–968.

[19] A. Liguori, M. Hakkarainen, Designed from biobased materials for recycling: Imine-based covalent adaptable networks, Macromol. Rapid Commun. 43 (13) (2022) 2100816.

[20] S.W. Zhou, C. Yu, M. Chen, C.Y. Shi, R. Gu, D.H. Qu, Self-healing and shape-shifting polymers controlled by dynamic bonds, Smart Molecules 1 (2) (2023) e20220009.

[21] C.J. Kloxin, C.N. Bowman, Covalent adaptable networks: smart, reconfigurable and responsive network systems, Chem. Soc. Rev. 42 (17) (2013) 7161–7173.

[22] X. Chen, M.A. Dam, K. Ono, A. Mal, H. Shen, S.R. Nutt, K. Sheran, F. Wudl, A thermally re-mendable cross-linked polymeric material, Science 295 (5560) (2002) 1698–1702.

[23] J. Canadell, H. Goossens, B. Klumperman, Self-healing materials based on disulfide links, Macromolecules 44 (8) (2011) 2536–2541.

[24] W. Post, A. Cohades, V. Michaud, S. Van Der Zwaag, S.J. Garcia, Healing of a glass fibre reinforced composite with a disulphide containing organic-inorganic epoxy matrix, Compos. Sci. Technol. 152 (2017) 85–93.

[25] C. Park, G. Kim, J.W. Jung, B. Krishnakumar, S. Rana, G.J. Yun, Enhanced self-healing performance of graphene oxide/vitrimer nanocomposites: A molecular dynamics simulations study, Polymer 206 (2020) 122862.

[26] I. Azcune, I. Odriozola, Aromatic disulfide crosslinks in polymer systems: Self-healing, reprocessability, recyclability and more, Eur. Polym. J. 84 (2016) 147–160.

[27] F. Zhou, Z. Guo, W. Wang, X. Lei, B. Zhang, H. Zhang, Q. Zhang, Preparation of self-healing, recyclable epoxy resins and low-electrical resistance composites based on double-disulfide bond exchange, Compos. Sci. Technol. 167 (2018) 79–85.

[28] G. Singh, V. Sundararaghavan, Modeling self-healing behavior of vitrimers using molecular dynamics with dynamic cross-linking capability, Chem. Phys. Lett. 760 (2020) 137966.

[29] C. Li, E. Jaramillo, A. Strachan, Molecular dynamics simulations on cyclic deformation of an epoxy thermoset, Polymer 54 (2) (2013) 881–890.

[30] N. Karak, Overview of Epoxies and Their Thermosets, Sustainable Epoxy Thermosets and Nanocomposites, ACS Publications, 2021, pp. 1–36.

[31] S. Kumar, S. Krishnan, K. Prabakaran, Renewable resource-based epoxy vitrimer composites for future application: A comprehensive review, ACS Sustain. Resour. Manage. 1 (9) (2024) 2086–2107.

[32] R. Gheisari, M. Vazquez, V. Tsigkis, A. Erdemir, K.L. Wooley, A.A. Polycarpou, Microencapsulated paraffin as a tribological additive for advanced polymeric coatings, Friction 11 (10) (2023) 1939–1952.

[33] N.J. Van Zee, R. Nicolaÿ, Vitrimers: Permanently crosslinked polymers with dynamic network topology, Prog. Polym. Sci. 104 (2020) 101233.

[34] M. Guerre, C. Taplan, J.M. Winne, F.E. Du Prez, Vitrimers: Directing chemical reactivity to control material properties, Chem. Sci. 11 (19) (2020) 4855–4870.

[35] Y. Yang, Y. Xu, Y. Ji, Y. Wei, Functional epoxy vitrimers and composites, Prog. Mater Sci. 120 (2021) 100710.

[36] BIOVIA, Materials Studio, 2017. http://www.3dsbiovia. com.

[37] H. Sun, S.J. Mumby, J.R. Maple, A.T. Hagler, An ab initio CFF93 all-atom force field for polycarbonates, J. Am. Chem. Soc. 116 (7) (1994) 2978–2987.

[38] S. Mazumder, N. Zhang, Cellulose–hemicellulose–lignin interaction in the secondary cell wall of coconut endocarp, Biomimetics 8 (2) (2023) 188.

[39] N. Zhang, Role of atomistic modeling in bioinspired materials design: A review, Comput. Mater. Sci 232 (2024) 112667.

[40] G.R. Harik, F.G. Lobo, D.E. Goldberg, The compact genetic algorithm, IEEE Trans. Evol. Comput. 3 (4) (1999) 287–297.

[41] W.G. Hoover, Canonical dynamics: Equilibrium phase-space distributions, Phys. Rev. A 31 (3) (1985) 1695.

[42] S. Plimpton, Fast parallel algorithms for short-range molecular dynamics, J. Comput. Phys. 117 (1) (1995) 1–19.

[43] A.P. Thompson, H.M. Aktulga, R. Berger, D.S. Bolintineanu, W.M. Brown, P. S. Crozier, P.J. In't Veld, A. Kohlmeyer, S.G. Moore, T.D. Nguyen, LAMMPS-a flexible simulation tool for particle-based materials modeling at the atomic, meso, and continuum scales, Comput. Phys. Commun. 271 (2022) 108171.

[44] A.M. Hubbard, Y. Ren, A. Sarvestani, D. Konkolewicz, C.R. Picu, A.K. Roy, V. Varshney, D. Nepal, Recyclability of Vitrimer materials: Impact of catalyst and processing conditions, ACS Omega 7 (33) (2022) 29125–29134.

[45] Y. Jin, Z. Lei, P. Taynton, S. Huang, W. Zhang, Malleable and recyclable thermosets: The next generation of plastics, Matter 1 (6) (2019) 1456–1493.

[46] A. Askadskii, Influence of crosslinking density on the properties of polymer networks, Polym. Sci. USSR 32 (10) (1990) 2061–2069.

[47] A. Bandyopadhyay, P.K. Valavala, T.C. Clancy, K.E. Wise, G.M. Odegard, Molecular modeling of crosslinked epoxy polymers: The effect of crosslink density on thermomechanical properties, Polymer 52 (11) (2011) 2445–2452.

[48] J. Chen, E.S. Garcia, S.C. Zimmerman, Intramolecularly cross-linked polymers: From structure to function with applications as artificial antibodies and artificial enzymes, Acc. Chem. Res. 53 (6) (2020) 1244–1256.

[49] C.W. Rajawasam, O.J. Dodo, M.S.N. Weerasinghe, I.O. Raji, S.V. Wanasinghe, D. Konkolewicz, N.D.A. Watuthanthrige, Educational series: Characterizing crosslinked polymer networks, Polym. Chem. 15 (4) (2024) 219–247.

[50] Y. Du, G. Zhao, G. Shi, Y. Wang, W. Li, S. Ren, Effect of crosslink structure on mechanical properties, thermal stability and flame retardancy of natural flavonoid based epoxy resins, Eur. Polym. J. 162 (2022) 110898.

[51] J. Fan, A. Anastassiou, C.W. Macosko, E.B. Tadmor, Molecular dynamics predictions of thermomechanical properties of an epoxy thermosetting polymer, Polymer 196 (2020) 122477.

[52] W.N. dos Santos, J. De Sousa, R. Gregorio Jr, Thermal conductivity behaviour of polymers around glass transition and crystalline melting temperatures, Polym. Test. 32 (5) (2013) 987–994.

[53] J. Dudowicz, K.F. Freed, J.F. Douglas, The glass transition temperature of polymer melts, J. Phys. Chem. B 109 (45) (2005) 21285–21292.

[54] G. Roudaut, D. Simatos, D. Champion, E. Contreras-Lopez, M. Le Meste, Molecular mobility around the glass transition temperature: A mini review, Innovative Food Sci. Emerg. Technol. 5 (2) (2004) 127–134.

[55] R. Xie, A.R. Weisen, Y. Lee, M.A. Aplan, A.M. Fenton, A.E. Masucci, F. Kempe, M. Sommer, C.W. Pester, R.H. Colby, Glass transition temperature from the chemical structure of conjugated polymers, Nat. Commun. 11 (1) (2020) 893.

[56] M.A. Islam, M.H. Mobarak, M.I.H. Rimon, M.Z. Al Mahmud, J. Ghosh, M.M. S. Ahmed, N. Hossain, Additive manufacturing in polymer research: Advances, synthesis, and applications, Polym. Test. 132 (2024) 108364.

[57] M. Du, H.A. Houck, Q. Yin, Y. Xu, Y. Huang, Y. Lan, L. Yang, F.E. Du Prez, G. Chang, Force–reversible chemical reaction at ambient temperature for designing toughened dynamic covalent polymer networks, Nat. Commun. 13 (1) (2022) 3231.

[58] Y. Yang, S. Zhang, X. Zhang, L. Gao, Y. Wei, Y. Ji, Detecting topology freezing transition temperature of vitrimers by AIE luminogens, Nat. Commun. 10 (1) (2019) 3165.

[59] K. Li, N.V. Tran, Y. Pan, S. Wang, Z. Jin, G. Chen, S. Li, J. Zheng, X.J. Loh, Z. Li, Next-generation vitrimers design through theoretical understanding and computational simulations, Adv. Sci. 11 (5) (2024) 2302816.

[60] J. Zheng, Z.M. Png, S.H. Ng, G.X. Tham, E. Ye, S.S. Goh, X.J. Loh, Z. Li, Vitrimers: Current research trends and their emerging applications, Mater. Today 51 (2021) 586–625.

[61] A. Klingler, D. Reisinger, S. Schlögl, B. Wetzel, U. Breuer, J.-K. Krüger, Vitrimer transition phenomena from the perspective of thermal volume expansion and shape (in) stability, Macromolecules 57 (9) (2024) 4246–4253.
[62] Z. Chen, Q. Shi, X. Kuang, H.J. Qi, T. Wang, Ultrastrong intrinsic bonding for thermoset composites via bond exchange reactions, Compos. B Eng. 194 (2020) 108054.
[63] W. Yang, X. Luo, J. Liu, J. Chen, X. Wu, Z. Fink, C. Shi, W. Zhong, C. Wang, L. Ying, Dynamic disulfide bond networks enable self-healable and mechanically resilient intrinsically stretchable organic solar cells, Energ. Environ. Sci. 18 (13) (2025) 6597–6607.
[64] M.A. Hagras, M.A. Bellucci, G. Gobbo, R.A. Marek, B.L. Trout, Computational modeling of the disulfide cross-linking reaction, J. Phys. Chem. B 124 (44) (2020) 9840–9851.
[65] J.M. Matxain, J.M. Asua, F. Ruipérez, Design of new disulfide-based organic compounds for the improvement of self-healing materials, PCCP 18 (3) (2016) 1758–1770.
[66] W. Nie, J.F. Douglas, W. Xia, Competing effects of molecular additives and cross-link density on the segmental dynamics and mechanical properties of cross-linked polymers, ACS Eng. Au 3 (6) (2023) 512–526.
[67] H.B. Seresht, M.S. Aghajanzadeh, R. Imani, M. Haghbin Nazarpak, Structural relaxation in a Schiff base-crosslinked aldehyde modified xanthan gum/gelatin hydrogel: Experimental and numerical validation using linear poroelasticity model, Polym. Adv. Technol. 35 (4) (2024) e6402.
[68] M. Sohrabian, M. Vaseghi, S.R. Eslamloo, M. Sameezadeh, B. Arab, F. Moradi, Molecular dynamics study on mechanical properties of polycaprolactone/bioactive glass nanocomposites, Comput. Mater. Sci 243 (2024) 113098.
[69] A. Esmaeili, A. Kuhzadmohammadi, M. Safarabadi, An analytical approach for the near-tip field around V-notch in orthotropic materials, Fatigue Fract. Eng. Mater. Str. 48 (1) (2025) 487–501.
[70] A.H. Barber, S.R. Cohen, S. Kenig, H.D. Wagner, Interfacial fracture energy measurements for multi-walled carbon nanotubes pulled from a polymer matrix, Compos. Sci. Technol. 64 (15) (2004) 2283–2289.
[71] T. Tsuda, T. Ogasawara, F. Deng, N. Takeda, Direct measurements of interfacial shear strength of multi-walled carbon nanotube/PEEK composite using a nano-pullout method, Compos. Sci. Technol. 71 (10) (2011) 1295–1300.